THE JOURNAL OF PHYSICAL CHEMISTRY C

Article

pubs.acs.org/JPCC

Dissecting the Effect of Morphology on the Rates of Singlet Fission: Insights from Theory

Xintian Feng,[†] Anatoly B. Kolomeisky,[‡] and Anna I. Krylov*,[†]

[†]Department of Chemistry, University of Southern California, Los Angeles, California 90089-0482, United States

[‡]Department of Chemistry, Rice University, Houston, Texas 77251-1892, United States

Supporting Information

ABSTRACT: The effect of morphology on singlet fission (SF) efficiency was investigated by using a combination of high-level electronic structure methods and a simple three-state kinetic model. The calculations reproduce the observed differences in SF efficiency in different polymorphs of 1,3-diphenylisobenzofuran (DPBF) and 1,6-diphenyl-1,3,5-hexatriene (DPH), as well as make predictions about 5,12-diphenyltetracene (DPT). The analysis of different factors contributing to the rates reveals that (i) there is more than one pair of adjacent chromophores that contribute to SF; (ii) not only slip-stacked configurations show efficient fission; and (iii) both electronic couplings and energy differences are responsible for different rates. The model predicts that the difference in SF efficiency in DPBF and DPH polymorphs increases at low temperature. In contrast, temperature dependence of the relative rates in the two DPT forms is predicted to be small. Our model predicts similar rates for the two polymorphs of DPT, although one form features much more favorable electronic couplings. This prediction depends strongly on the magnitude of Davydov's splitting; small changes in its value may change the ratio in favor of faster SF in xylene-grown crystals of DPT.

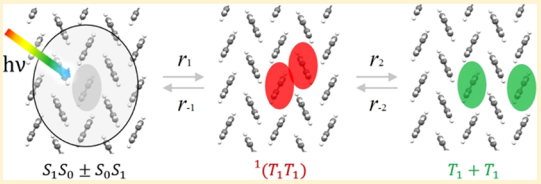

1. INTRODUCTION

Singlet fission (SF), a process in which one singlet excited state is converted into two coupled triplet states, is of interest in the context of organic solar cell technology.[1,2] Although the phenomenon has been known for quite some time,[3] the mechanistic details are still unclear. Thus, despite vigorous research,[1,2] the design principles for materials capable of efficient SF remain elusive.

Many theoretical studies of SF interrogated electronic structure aspects of the problem[1,2,4−14] focusing on energies of the relevant states and estimating electronic couplings using diabatization schemes or one-electron approximations. Several studies attempted to estimate the rates of SF by using simple Landau−Zener type of approaches[7] or more sophisticated dynamics simulations.[15−17] Recently, we introduced a theoretical framework[18,19] that combines high-level ab initio calculations of electronic factors with a simple 3-state kinetic model of the SF process. Our approach is based on correlated adiabatic wave functions and the respective transition density matrices that give rise to nonadiabatic couplings. The model was used to explain the observed trends in SF rates in acenes and to interrogate the relative importance of electronic and entropic contributions.[19] A kinetic model for the first step of singlet fission, the generation of the multiexciton state, has been developed by Van Voorhis and co-workers;[20] their approach is based on a Marcus-like rate expression and employs constrained density functional theory (DFT)[21] for calculations of the diabatic and adiabatic states and the couplings.

Several factors contribute to the efficiency of SF. First, the individual chromophores should have properly aligned energy levels, such that $E(S_1) \approx 2 \times E(T_1)$. Second, the interaction between the chromophores in a molecular solid is also critically important. The arrangement of the molecules in a solid affects the energy levels, the exciton delocalization, and the electronic couplings between the relevant states. Although the significance of each of these factors for the SF process is obvious, it is not clear what exactly is the best arrangement. Several recent experimental studies have illustrated the significance of the morphology on the rates and yields of SF.[4,22−28] For example, covalently linked dimers of tetracene show significantly decreased rates and yields.[22] Likewise, SF is much slower in solution than in the bulk.[29] While these observations can be explained by unfavorable couplings and entropic contributions,[19] the reported differences in the yields of SF in different forms of the same molecular solid[25−28] are more puzzling. Several examples are listed below. Efficient SF has been reported in amorphous 5,12-diphenyltetracene (DPT); however, the crystalline form shows no fission.[23] Bardeen and co-workers reported a 1.5 difference in SF rates in the two polymorphs of 1,6-diphenyl-1,3,5-hexatriene (DPH). Finally, recent studies by Michl and co-workers[25−27] presented strikingly different yields (and rates) in the two forms of 1,3-diphenylisobenzofuran (DPBF): while the so-called α form shows 125% yield of triplet excitons (at 300 K), the second form, β, shows <10%. The difference becomes even more pronounced at low temperature. The structural, spectroscopic,

Received: June 15, 2014
Revised: August 3, 2014
Published: August 7, 2014

   dx.doi.org/10.1021/jp505942k | J. Phys. Chem. C 2014, 118, 19608−19617

and physical properties of the two forms are similar; the calculations reported in ref 26 further confirmed that the electronic structure of the two polymorphs is indeed very similar.

In this work, we investigate three systems: DPBF, DPH, and DPT. We explain the observed differences in the SF efficiency in DPBF and DPH by using our recently developed theoretical framework.[18,19] We also make predictions about SF rates in the two crystalline forms of DPT.[23,30]

2. THEORETICAL FRAMEWORK

Figure 1 summarizes relevant electronic states and salient features of our model (see refs 18 and 19 for details). SF is

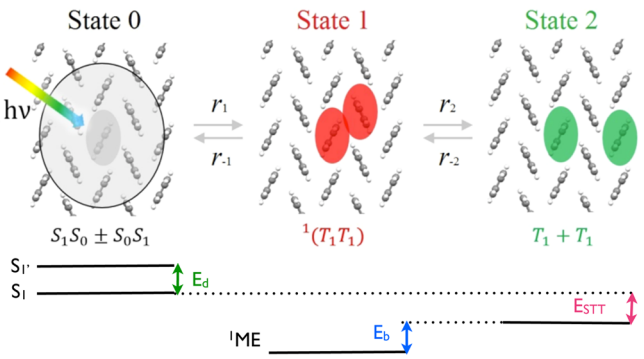

Figure 1. Three-state model of singlet fission. "State 0" denotes an initially excited delocalized state, "State 1" is a multiexciton state, $^1T_1(A)T_1(B)$, and "State 2" corresponds to two independent triplets. Relevant electronic energies are $E_{stt} = E[S_1] - 2 \times E[T_1]$, multiexciton stabilization energy, $E_b = E[^5ME] - E[^1ME]$, and Davydov's splitting $E_d = E[S_{1'}] - E[S_1]$.

initiated by the absorption of a photon producing an initially excited delocalized singlet state. In a dimer, its wave function can be described as a linear combination of the excitonic ($S_1(A)S_0(B)$ and $S_0(A)S_1(B)$) and charge-resonance (A^-B^+ and A^+B^-) configurations:

$$c_1S_1(A)S_0(B) + c_2S_0(A)S_1(B) + c_3A^-B^+ + c_4A^+B^- \quad (1)$$

The oscillator strength is spread over several such excitonic states (two in the dimer, denoted by $S_1(AB)$ and $S_{1'}(AB)$, following the notations from ref 18); their energies differ by the so-called Davydov splitting, E_d. We assume that the initially excited state relaxes to the lowest excitonic singlet state prior to SF; thus, in our calculations we use energy and electronic coupling of the lowest excitonic state of a dimer, whether it happens to be bright or dark. In the case when the Davydov splitting is small, giving rise to substantial thermal populations of the higher states, we include the respective rates into the total rate calculation using Boltzmann's weights:

$$BF \equiv P(S_1)/P(S_{1'}) = e^{\beta E_d} \quad (2)$$

State 1 is the multiexciton state (^1ME); it can be described as two triplet states localized on the adjacent individual chromophores coupled into a singlet state, $^1T(A)T(B)$. State 2 is two uncoupled triplets.

Recently, we introduced a simple three-state model for the rate of SF process.[19] The electronic energy diagram is shown in Figure 1. The relevant energies are E_{stt} (the difference between the initial singlet state and two independent triplets, $E_{stt} = E[S_1] - 2 \times E[T_1]$) and E_b (multiexciton stabilization energy, $^5ME-^1ME$). The rates of the first (state 0 → state 1) and the second (state 1 → state 2) steps are denoted by r_1/r_{-1} and r_2/r_{-2} (note that these notations differ from the Merrifield triplet recombination model[31]). This minimalist model of SF can be further extended by including the decay channel (characterized by rate r_d), as discussed below.

Using a linear free energy approach,[32,33] which argues that the activation energy for a process is proportional to the free energy difference of the reaction, one can connect the rates and the free energies of the three states:

$$G_0 = 0 \quad (3)$$

$$G_1 = -E_{stt} - E_b - TS_1 \quad (4)$$

$$G_2 = -E_{stt} - TS_2 \quad (5)$$

where TS_1 and TS_2 denote entropic contributions (relative to State 0) to the Gibbs free energies of states 1 and 2. This model is, admittedly, very simple and relies on numerous approximations; its validity will be judged by a careful comparison with the experimental trends. We note that the linear free energy approach has been successfully utilized to rationalize and predict trends in a large variety of processes in organic chemistry, giving rise to such important relationships as Hammett, Taft, Grunwald–Winstein, Swain–Scott, and Bronsted scales.[32,33] Recently, the assumptions behind linear free energy relationships have been analyzed and justified by first-principle calculations for a series of S_{N2} reactions.[34] The linear free energy approach works the best when applied to a series of sufficiently similar compounds/processes. Because the polymorphs of molecular solids have very similar structural and physical properties, this is a good case for applying a linear free energy relationship.

The entropy is crucially important for singlet fission;[19,35] for example, it allows one to overcome an unfavorable electronic energy difference in tetracene. Entropy also facilitates the separation of the two bound triplets (multiexciton state, ^1ME) into two independent triplets. In solids, the entropy increases both in the first ($S_1 \rightarrow {}^1ME$) and in the second ($^1ME \rightarrow 2T_1$) steps.[19] In our previous work,[19] we estimated the entropic contributions for crystalline acenes. The calculation depends on the degree of the delocalization of state 0; thus, the magnitude of entropic contribution depends on the morphology. However, when comparing rates in homologically similar compounds (such as acenes) or polymorphs of the same compound, it is reasonable to assume that the entropic contributions are similar because (i) the number of the nearest neighbors is the same for the polymorphs considered in the present paper; (ii) the lattice parameters and, consequently, the average separation between the chromophores are very close; and (iii) the spectroscopic properties of different forms are very similar, suggesting a similar degree of delocalization of the initial exciton. Under this assumption, the relative rates are determined by the electronic energy differences alone (and, of course, the couplings).

In the present study we focus on estimating the rate of the first step, $S_1(AB) \rightarrow {}^1ME$ and $S_{1'}(AB) \rightarrow {}^1ME$:

$$r_1[S_1(AB) \rightarrow {}^1ME] \approx \left(\frac{\|\gamma\|}{E_{stt} + E_b}\right)^2 e^{\alpha\beta(E_{stt}+E_b)} \quad (6)$$

dx.doi.org/10.1021/jp505942k | J. Phys. Chem. C 2014, 118, 19608–19617

$$r_1[S_{1'}(AB) \rightarrow^1 ME] \approx \left(\frac{\|\gamma'\|}{E_{stt} + E_b + E_d}\right)^2 e^{\alpha\beta(E_{stt}+E_b+E_d)} \quad (7)$$

where α is a proportionality coefficient (we use 0.5, as in the previous study[19]) and $\beta = 1/kT$. $\|\gamma\|$ and $\|\gamma'\|$ are the norms of symmetrized one-particle transition density matrices between $^1ME-S_1$ and $^1ME-S_{1'}$, respectively. $(\|\gamma\|/\Delta E)$ is a proxy for a nonadiabatic matrix coupling element (see refs 18 and 36 for details and benchmarks); the rate is proportional to its square, as follows from the Fermi Golden Rule expression for rates of nonadiabatic transitions. The overall rate is computed as Boltzmann-averaged r_1 and r_1':

$$r = \frac{BF \cdot r_1[S_1 \rightarrow^1 ME] + r_1[S_{1'} \rightarrow^1 ME]}{BF + 1} \quad (8)$$

where BF is defined by eq 2.

We note that $\|\gamma\|$ is not equivalent to the coupling; thus, it cannot be used to compute absolute rates of nonadiabatic transitions. However, it contains information about state interactions (e.g., mixing of CR configurations into the S_1 and ME states), and the changes in $\|\gamma\|$ along different displacements correlate well with the magnitude of the full nonadiabatic coupling, as illustrated by a recent benchmark study.[36]

Finally, we note that the rates are computed for fixed geometries of dimers taken from the crystal structures; thus, the effect of nuclear motions is not included. While it may be important for absolute rate calculations, we expect that the frequencies of the promoting modes are similar in the polymorphs, leading to the cancellation of the Golden Rule like prefactors in the rate expressions. This limitation can be lifted by including classical or quantum estimates of Franck–Condon factors.[37−39]

In ref 19, this 3-state model was used to to compute the first-passage time,[40] τ:

$$\tau = \frac{1}{r_1} + \frac{1}{r_2} + \frac{r_{-1}}{r_1 r_2} = \frac{1}{r_1} + \frac{1}{r_2}\left(1 + \frac{1}{K_1^{eq}}\right) \quad (9)$$

Note that this minimalist model focuses on the rates alone and does not describe yields. Efficient SF can be identified by small τ that reduces the losses due to the competing channels (radiationless or radiative relaxation, exciton trapping, etc.). To make a more quantitative connection between the rates and the experimental yields, we extend the model by introducing decay channels (from state 0 and state 1) characterized by rate r_d. For simplicity, we assume the same yields ($Y_2 = Y_1$) for steps 1 and 2:

$$Y = Y_1 Y_2 = (Y_1)^2 = \left(\frac{r_1}{r_1 + r_d}\right)^2 = \left(\frac{1}{1 + x}\right)^2 \quad (10)$$

where

$$x = \frac{r_d}{r_1} \quad (11)$$

describes the competition between the decay and SF rates: when $r_d \ll r_1$, $Y_1 \approx 1$. The effective rate of the first step is also affected by the decay, because the residence time in state 0 is now equal to

$$\tau_1 = \frac{1}{r_1 + r_d} \quad (12)$$

Thus, the rate of the first step that takes into account the decay channel, r_1^d, can be written as

$$r_1^d = r_1(1 + x) \quad (13)$$

Note that, while lowering the yield, the decay accelerates the effective rate out of state 0. In section 4.1, we use experimental data on the yields of SF in DPBF to evaluate x. We then use x to evaluate r_1^d. The assumption of equal yields is, of course, very crude and is used here only to illustrate the overall effect of the decay channel. It can be relaxed and refined when more detailed experimental data becomes available.

3. COMPUTATIONAL DETAILS

We use the RAS-2SF method,[41,42] which is capable of describing both the excitonic and multiexciton states in the same framework. Following the protocol developed in ref 19, we employ the cc-pVTZ basis[43] from which f-functions were removed, cc-pVTZ(-f). RAS-2SF calculations are performed using the ROHF quintet reference and use 4-electrons-in-4-orbitals active space.

The structures of different forms of crystalline DPBF, DPH, and DPT are taken from refs 23, 26, 28, and 30. From these structures, we selected monomers and dimers for electronic structure calculations, as described in the respective sections below. We also performed geometry optimizations for the monomers at the RI-MP2/cc-pVTZ level of theory; at these structures RAS-SF vertical excitation energies were computed and compared with the experimental data in solutions. All relevant Cartesian geometries are given in the Supporting Information.

All calculations are performed using the Q-Chem electronic structure package.[44,45] The computed adiabatic wave functions are used to calculate one-particle density matrices and, consequently, to estimate nonadiabatic coupling elements, as described in ref 18. While RAS-2SF produces qualitatively correct wave functions, the absolute excitation energies are not sufficiently accurate, due to the lack of dynamic correlation. Consequently, energies of the excitonic states are overestimated; thus, S_1-^1ME gaps are of poor quality. However, energy differences such as Davydov splittings and multiexciton stabilization energy are reproduced much better due to error cancellation, as confirmed by comparisons with higher-level methods, such as SOS-CIS(D) (see the Supporting Information of ref 18). To obtain better estimates of the S_1-^1ME gaps, we use an empirical correction based on the experimental excitation energies of the individual chromophores:

$$E_{stt}^{corr} = E_{stt}^{comp} + (\Delta E[S_1] - 2 \times \Delta E[T_1]) \quad (14)$$

$$\Delta E[S_1] = E^{exp}[S_1] - E^{comp}[S_1] \quad (15)$$

$$\Delta E[T_1] = E^{exp}[T_1] - E^{comp}[T_1] \quad (16)$$

Note that, while these energy gaps are crucially important for absolute rates or when comparing the rates in different compounds, in the calculations of the relative rates of the polymorphs of the same compound, the correction (almost) entirely cancels out, as one can see from eq 6.

When calculating couplings from $\|\gamma\|$ and ΔE, it is more appropriate to use an unshifted value of E_{stt}, as it is consistent with the Hamiltonian that defines nonadiabatic coupling. All

dx.doi.org/10.1021/jp505942k | J. Phys. Chem. C 2014, 118, 19608−19617

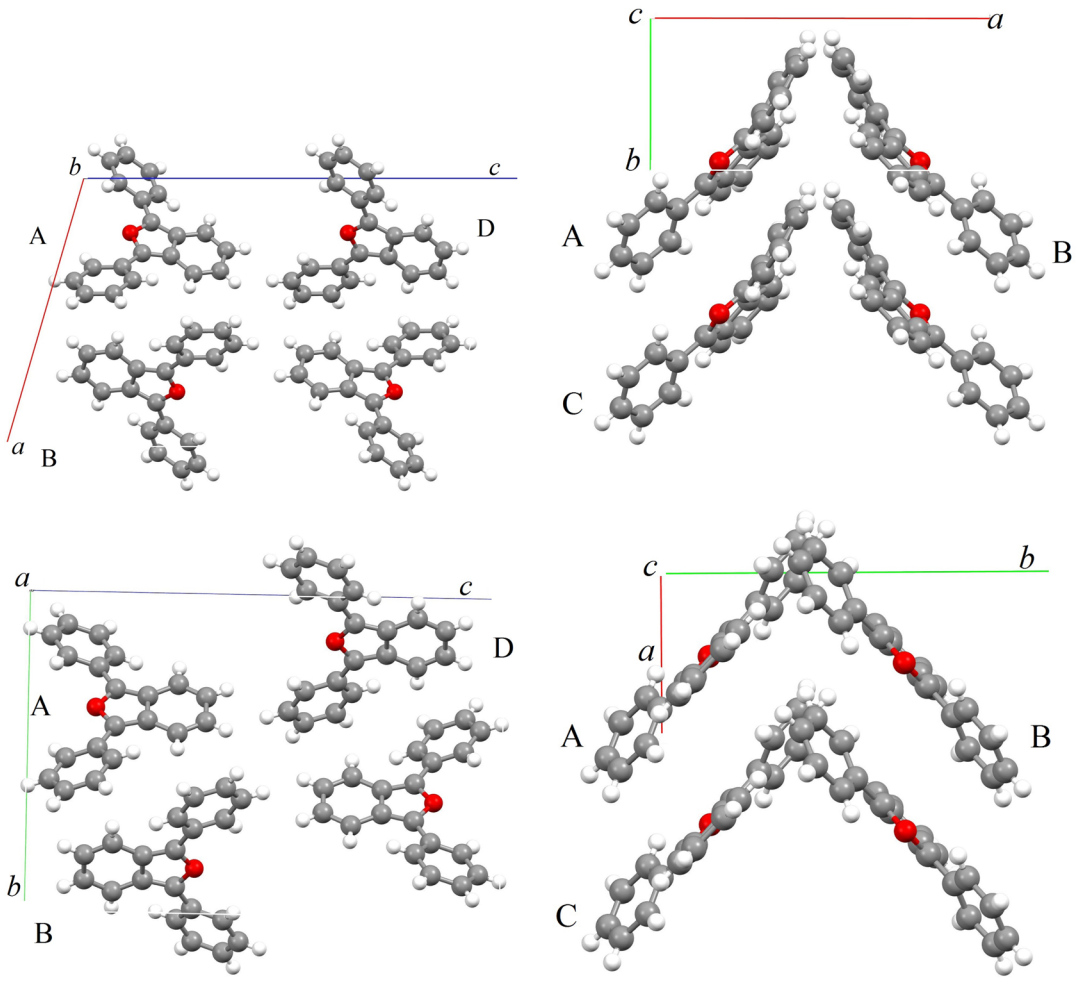

Figure 2. Structure of DPBF. Unit cells of the α (top left, view along b-axis; top right, view along c-axis) and β (bottom left, view along a-axis; bottom right, view along c-axis) polymorphs. Dimers considered in rate calculations: dimer1 (A + C), dimer2 (A + B), dimer3 (A + D), dimer4 (B + C), and dimer5 (B + D).

calculations presented in the main manuscript use unshifted E_{stt} in the couplings calculations. In this case, the energy corrections exactly cancel out from the relative rate calculations, that is, relative rates do not depend on the absolute values of E_{stt} but only on their differences. We expect that the differences in E_{stt} between different dimer structures of the same compound are reproduced much better than the respective absolute values. In the Supporting Information, we also present values computed with couplings with the shifted gap (this leads to a small change in the relative rates).

4. RESULTS AND DISCUSSION

4.1. 1,3-Diphenylisobenzofuran. Figure 2 shows the structure of DPBF. The main structural differences between the α and β forms are the length of the c-axis (20.271 and 19.423 Å in the α and β forms, respectively) and angle β (106.215° and 93.534°) of the unit cell, as shown in Figure 2. In our calculations, we consider five different dimers: dimer1 is A + C, dimer2 is A + B, dimer3 is A + D, dimer4 is B + C, and dimer5 is B + D. There are the same number of dimers of type 1, 2, and 3 and twice as many dimers of type 4 and 5 (dimers are counted by considering different types of nearest neighbors for each molecule in the unit cell).

Table 1 summarizes relevant electronic factors, E_{stt} (corrected), E_b, E_d, $\|\gamma\|$, and $\|\gamma'\|$; the respective raw energies are given in the Supporting Information (Table S1).

Table 1. Relevant Electronic Energies (eV) and $\|\gamma\|^2$ in Several DPBF Dimers

structure		E_{stt}	E_b	E^d	$\|\gamma\|^2$	$\|\gamma'\|^2$
dimer 1	α	−0.494	0.006	0.002	0.008	0.006
	β	−0.518	0.005	0.002	0.008	0.005
dimer 2	α	−0.506	0.003	0.141	0.003	8.3×10^{-4}
	β	−0.533	0.003	0.144	0.003	7.2×10^{-4}
dimer 3	α	−0.462	0.000	0.008	0.018	0.014
	β	−0.485	0.000	0.011	8.5×10^{-6}	8.5×10^{-6}
dimer 4	α	−0.467	0.000	0.016	4.7×10^{-5}	4.7×10^{-5}
	β	−0.492	0.000	0.017	4.0×10^{-5}	4.0×10^{-5}
dimer 5	α	−0.474	0.000	0.032	1.7×10^{-6}	7.8×10^{-7}
	β	−0.493	0.000	0.020	1.1×10^{-6}	1.2×10^{-6}

We observe that, in all dimers, SF is more endothermic (by ~0.02 eV) in the β form. In agreement with calculations from ref 26, we observe the largest Davydov splitting in dimer2. In both dimer1 and dimer2, the couplings are larger for the S_1 state than for $S_{1'}$. The magnitudes of the couplings in the two forms of dimer1 and dimer2 are similar. Interestingly, dimer3

dx.doi.org/10.1021/jp505942k | J. Phys. Chem. C 2014, 118, 19608−19617

Table 2. Relative Rates Computed for Different Dimers from α and β Forms; 1:2:3:4 Denotes Relative Rates in Dimers1−4 (See Fig. 2 for Definitions of the Dimers)

form	dimer	$S_1 \rightarrow {}^1$ME rate	$S_{1'} \rightarrow {}^1$ME rate	Boltzmann factor	total rate
			T = 298 K		
α	1:2:3:4	3.37:1:11.5:0.028	0.98:1:3.81:0.014	1.1/247/1.4/1.9	2.99:1:10.8:0.03
β	1:2:3:4	3.47:1:0.06:0.024	0.95:1:0.003:0.013	1.1/277/1.5/1.9	2.86:1:0.0068:0.03
α/β	1	1.48:1	1.77:1		1.59:1
α:β	2	1.52:1	1.71:1		1.52:1
α/β	3	3 048:1	2274:1		2702:1
α/β	4	1.76:1	1.73:1		1.76:1
α/β	all	5.34:1	5.03:1		5.77:1
			T = 77 K		
α	1:2:3:4	7.94:1:119:0.217	1:1 201:24:0.102	1.4/2.4 × 10^9/3.4/11.6	7:49:1:129:0.256
β	1:2:3:4	9.15:1:0.074:0.210	1:1320:0.025:0.110	1.4/3.8 × 10^9/5.4/13.5	8.07:1:0.089:0.246
α/β	1	6.15:1	7.39:1		6.58:1
α/β	2	7.09:1	6.73:1		7.09:1
α/β	3	11 300:1	7 118:1		10 400:1
α/β	4	7.34:1	6.82:1		7.38:1
α:β	all	81.3:1	6.71:1		96.8:1

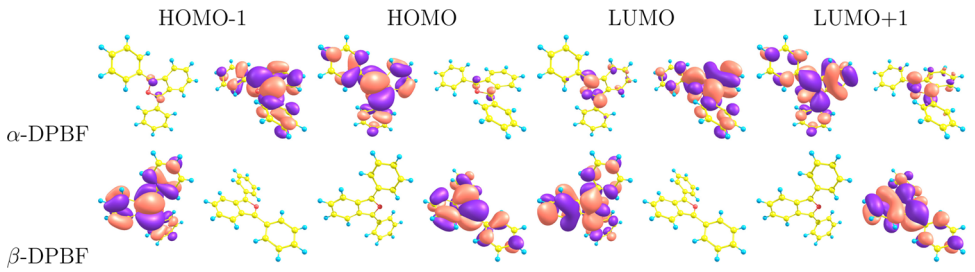

Figure 3. Active-space molecular orbitals from RAS-2SF calculations of dimer3 in the two polymorphs. Top, α-DPBF; bottom, β-DPBF. From left to right: HOMO−1, HOMO, LUMO, LUMO+1; contour value 0.02.

(whose structure is neither stacked nor herringbone like) shows the largest difference between the two polymorphs as well as the largest coupling (for the α form). Dimer4 and dimer5 feature smaller couplings (dimer5 is excluded from the rate calculations below). Note that the trends in Davydov splitting and E_b do not follow the trends in $\|\gamma\|$, e.g., E_b is zero for dimer3, which has the largest coupling. This observation further illustrates the importance of computing the coupling, rather than using energy differences as a proxy.

On the basis of Davydov's splittings, for dimer1 and dimer3 both singlet states should be included in the rate calculations at room temperature (Boltzmann factors are 1−1.5), whereas for dimer2 only the lowest excitonic state should be considered. At lower temperatures, however, the contributions from the higher excitonic states become insignificant.

Table 2 summarizes the results for rate calculations and the respective Boltzmann factors. First, for each form, we compute the rates relative to the dimer2 rate. Then for each dimer, we compute the relative rates for the α and β forms. As one can see, dimer3 shows the fastest rate in the α form for both S_1 and $S_{1'}$. In β, dimer1 and dimer2 contribute the most. At lower temperature, the differences are significantly enhanced due to the difference in E_{stt} between the two forms.

To compute relative rates, we add the rates for each type of dimer (multiplied by the number of the dimers of each type) for the α and β forms and then scale the result by the α/β ratio for dimer2 (the rates for each form are computed relative to dimer2). At 298 K, this yields

$$r_1(\alpha)/r_1(\beta) = (2.99 + 1 + 10.8 + 0.03 \times 2) \times 1.52 : (2.86 + 1 + 0.006 + 0.026 \times 2) = 5.8:1 \quad (17)$$

which is in semiquantitative agreement with the experimental ratio, 2.7 in bulk crystals and 3.4 in films.[25,26] We note that using Boltzmann averaging leads to a small but noticeable difference, e.g., the ratios computed only for the S_1 and $S_{1'}$ states are 5.3:1 and 5.0:1, respectively. At 77 K, the computed ratio is much larger: $r_1(\alpha)/r_1(\beta)$ = 97; this is because SF is more endothermic in the β form than in the α form. The experimental rates at lower temperature have not been reported; however, our result is in agreement with the observed increased difference in the SF efficiency, e.g., at 300 K, the yield of triplets is 125% and 10% for the α and β forms, respectively, whereas at 77 K, the yield for the α form increases up to 200%. The yield of triplets for the β form at 15 K is <5%.

Using the extension of the model described in section 2, eqs 10−13, the experimental total yields of triplets, Y, result in the following yields for step 1: $Y_1(\alpha)$ = 0.84 and $Y_1(\beta)$ = 0.22 at 298 K, and $Y_1(\alpha)$ = 1 and $Y_1(\beta)$ = 0.15 at 77 K. Note that the difference in yields Y_1 for the two forms (as well as differences at two different temperatures) are less pronounced than in the total triplet yields. Using these yields, we estimate the values of parameter x for the two forms by eq 11. At 298 K, $x(\alpha)$ = 0.27 and $x(\beta)$ = 3.5, and at 77 K, $x(\alpha)$ = 0 and $x(\beta)$ = 5.7. Now we can use these values of x derived from the experimental yields to correct the rates of the first step (or, more precisely, the rates out of state 0) to take into account the decay channel using eq

dx.doi.org/10.1021/jp505942k | J. Phys. Chem. C 2014, 118, 19608−19617

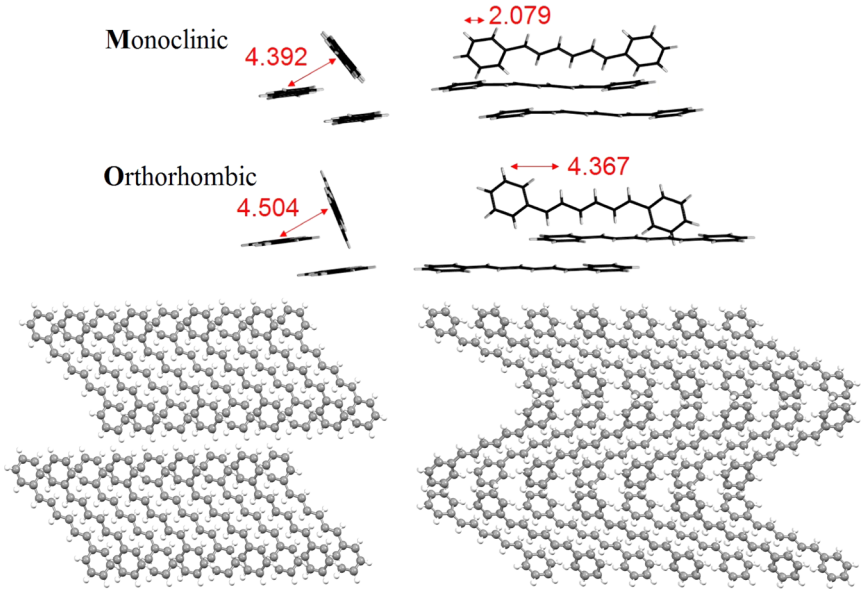

Figure 4. Structure of DPH. Top, monoclinic form (M-DPH); bottom, orthorhombic form (O-DPH).

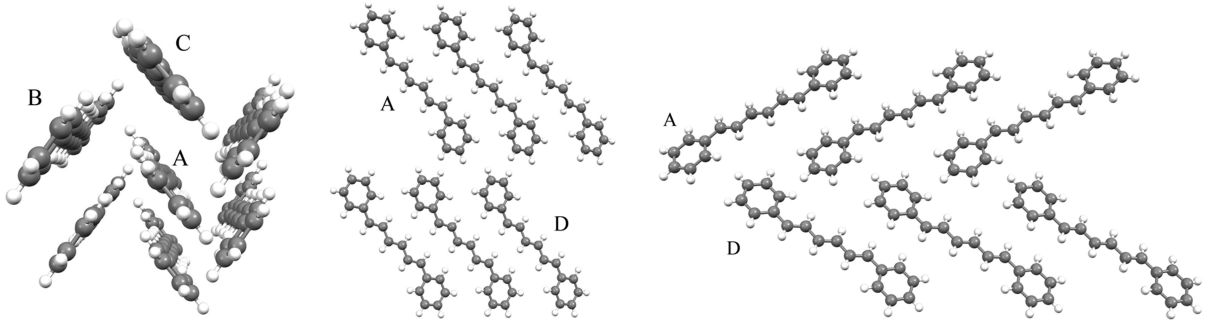

Figure 5. Four monomers from the crystal structure of DPH used in dimers' calculations. Four different dimers are considered: dimer1, A + B (left); dimer2, A + C (left); dimer3, A + D (middle, M form; right, O form).

13. At 298 K, we obtain $r_1^d(\alpha)/r_1^d(\beta)$ = 2.1:1, which is in a better agreement with the experiment than the r_1 values presented above. At 77 K, our calculations predict the following ratio: $r_1^d(\alpha)/r_1^d(\beta)$ = 14.5:1.

We emphasize that explicit values for the rate ratios depend on the yield in each step. However, for all conditions we expect that the decay processes will modify the rate for the α form much less than that of the β form because of the higher yield of the former.

In summary, our calculations explain the observed difference in rates and efficiency of SF in the two polymorphs of DPBF. The calculations also explain the larger difference at lower temperature. The analysis of different components attributes the difference to a particularly favorable chromophore arrangement in dimer3 of the α form, in contrast to the β form. The difference in rates of the two forms of dimer3 is dominated by the couplings and can be explained by more extensive orbital delocalization in the α form (see Figure 3); however, the energetic contribution is also important (SF is ∼0.02 eV less endothermic in the α form). The next significant contribution to the rate comes from dimer1. In this case, the α form is also more efficient than the β form; however, the difference is much smaller (1.5:1). In this case, the couplings are similar and the difference in rates is mostly due to different E_{stt}. This finding is in agreement with the conclusions from ref 20 that emphasized the importance of the overall thermodynamic drive (i.e., E_{stt}) for the fast singlet fission.

To better understand the nature of coupling, we analyzed the RAS-2SF wave functions of dimer1 and dimer3 following the same strategy as in ref 18 Leading electronic configurations of the ^{1}ME, ^{5}ME, and S_1 states are given in the Supporting Information (Tables S5−S8). As one can see, in both forms ^{5}ME state is of purely multiexciton character and does not include CR contributions. However, in dimer3 the ^{1}ME state has ∼30% of CR character in the α form and no CR character in the β form. The S_1 state of dimer3 shows a small admixture (2%) of CR configurations in the α form. Interestingly, dimer1's states show no CR character in either form, which is consistent with the smaller magnitude of the couplings. Thus, the α form of dimer3 has the largest couplings because of the efficient mixture of CR configurations into the ^{1}ME state.

4.2. 1,6-Diphenyl-1,3,5,-hexatriene. Figure 4 shows the structure of the two polymorphs of DPH, monoclinic form and orthorhombic form; Figure 5 shows the individual chromophores used to construct different dimers. We considered three types of dimers: dimer1 is A + B (herringbone-like structure, as in acenes), dimer2 is A + C (stacked structure), and dimer3 is A + D (in-plane nonstacked structure). There are four dimer1s, two dimer2s, and two dimer3s, which will be taken into account in the overall rate calculation. As explained above, the dimers

dx.doi.org/10.1021/jp505942k | J. Phys. Chem. C 2014, 118, 19608−19617

are counted by considering different types of nearest neighbors for each molecule in the unit cell.

Table 3 summarizes relevant energies (the raw values are given in the Supporting Information, Table S9). In this case,

Table 3. Relevant Electronic Energies (eV) and $\|\gamma\|^2$ in Several DPH Dimers

structure	form	E_{stt}	E_b	E^d	$\|\gamma\|^2$
dimer1	M	−0.108	0.015	0.443	0.104
	O	−0.106	0.008	0.192	0.018
dimer2	M	0.044	0.006	0.145	0.001
	O	−0.082	0.009	0.197	0.006
dimer3	M	0.102	0.000	0.117	2.3×10^{-5}
	O	−0.040	0.000	0.123	4.0×10^{-4}

Davydov's splitting is sufficiently large for all three dimers, such that only the $S_1 \rightarrow {}^1$ME rate needs to be considered. The results of rate calculations are given in Table 4. We note that

Table 4. Relative Rates Computed for Different Dimers from M and O Forms of DPH; 1:2:3 Denotes Relative Rates in Dimers1−3 (See Fig. 5 for Definitions of Different Dimers)

form	dimer	$S_1 \rightarrow {}^1$ME Rate
	298 K	
M	1:2:3	1.98:1:0.111
O	1:2:3	1.53:1:0.153
M/O	1	6.56:1
M/O	2	5.07:1
M/O	3	3.67:1
M/O	all	6.10:1
	200 K	
M	1:2:3	0.50:1:0.18
O	1:2:3	1.20:1:0.21
M/O	1	6.88:1
M/O	2	16.5:1
M/O	3	14.3:1
M/O	all	9.96:1
	100 K	
M	1:2:3	0.008:1:0.83
O	1:2:3	0.58:1:0.55
M/O	1	7.96:1
M/O	2	590:1
M/O	3	892:1
M/O	all	401:1

dimer1 (whose structure is similar to the herringbone structure of dimers from acenes) provides dominant contributions in both M and O at 298 K. Dimer2 (stacked structure) follows dimer1 closely (at 298 K). Dimer3 shows small contributions at room temperature. In dimer1, E_{stt} is nearly the same in both forms; thus, the difference in rates is dominated by the coupling. The situation is different in dimer2 and dimer3 where SF is exothermic in M and endothermic in O.

Differences in couplings in dimer1 from the M and O crystals can be rationalized based on the results of ref 18, where the effects of orientation were investigated for model acenes structures. Figure 6 shows the $S_1-{}^1$ME coupling along the interfragment slipping coordinate (D, the displacement along the long molecular axis). As observed in ref 18, γ varies strongly along this coordinate. As clearly seen from Figure 6, γ drops by a factor of 2 as D varies from 2.1 Å (its value in M-DPH) to 4.4

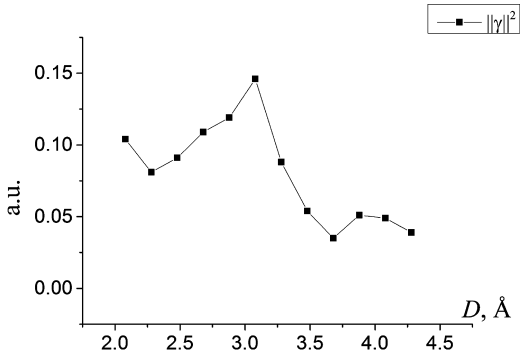

Figure 6. $\|\gamma\|^2$ for dimer1 of M-DPH as a function of displacement D along the long molecular axis. D = 2.079 Å in M-DPH and 4.367 Å in O-DPH (see Figure 4).

Å (the value of D in O-DPH). Thus, it is the difference in the slipping coordinate of the two forms, rather than the distance between the planes of the chromophores, that controls the coupling. The MOs of the two forms are shown in the Supporting Information (Figure S1); M-DPH shows larger delocalization. The wave function analysis of the ME and S_1 states of dimer1 (see Supporting Information, Tables S11−S12) reveals that the weights of CR configurations are almost twice higher in the M form, i.e., the ^{1}ME and S_1 states have 21% and 9% of CR character in M, whereas in the O form the CR weights in these states are only 12% and 4%. Thus, as in the case of dimer3 of DPBF, larger couplings in dimer1 of M-DPH are due to a noticeable mixing of the CR configurations into the ^{1}ME state.

Using the same algorithm and assuming that all dimers are equal, we obtain $r_1(M)/r_1(O)$ = 6.1:1 (at 298 K), which is in semiquantitative agreement with the experimental ratio of 1.5:1. As seen from Table 4, all dimers exhibit a similar trend, but for different reasons: in dimer1, couplings are responsible for faster rate in the M form, whereas in dimer2 and dimer3, E_{stt} drive the difference. At lower temperatures, we observe the change in the relative contributions of dimer1, dimer2, and dimer3. Our calculations predict an increased difference in rates between the two forms at low temperature.

4.3. 5,12-Diphenyltetracene. DPT is a promising SF system. Interestingly, an amorphous DPT film shows a high triplet quantum yield of 122% (ref 23), whereas a vapor-grown DPT crystal shows almost no SF (Bradforth, private communication 2014).

Two different crystal structures of DPT have been reported: a crystal grown by vacuum sublimation[23] and from xylene solvent.[30] Figure 7 shows representative dimer structures taken from the two X-ray structures (V and X, respectively) and the three dimers used in the rate calculations. The relevant electronic properties are collected in Table 5; raw energies are given in the Supporting Information (Table S14). Dimer1 and dimer2 are slip-stacked; dimer3 is not. There is an equal number of the dimers of type 1 and 2, and 4 times as many of dimer3. Note that in dimer1 and dimer2 in V, the DPT moieties are offset by 0.5 and 1.5 rings, respectively, whereas in X the chromophores are offset by 0.25 and 2 rings. As observed for all acenes in ref 18, half-integer ring offset structures feature small $\|\gamma\|$ and large $\|\gamma'\|$, whereas structures offset by the integer number of rings have large $\|\gamma\|$ and small $\|\gamma'\|$. The results for dimer1 and dimer2 in Table 5 follow this trend. The small magnitude of couplings (between the ^{1}ME−S_1 pair) in all

dx.doi.org/10.1021/jp505942k | J. Phys. Chem. C 2014, 118, 19608−19617

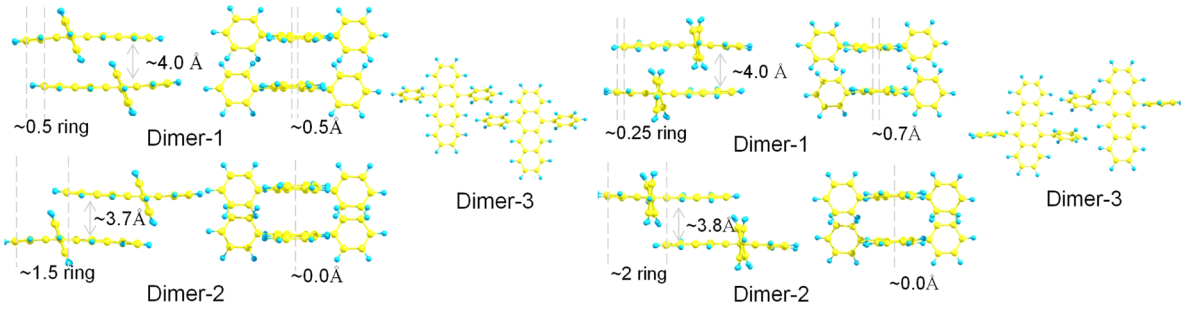

Figure 7. Crystal structure of DPT. Left, Three dimers from DPT crystal grown by vacuum sublimation (V); right, three dimers from DPT crystal grown from xylene solvent (X).

Table 5. Relevant Electronic Energies (eV) and Couplings in Several DPT Dimers

structure	form	E_{stt}	E_b	E^d	$\|\gamma\|$	$\|\gamma'\|$
dimer1	V	0.590	0.004	0.202	0.001	0.093
	X	0.615	0.014	0.374	0.118	0.029
dimer2	V	0.711	0.025	0.004	0.001	0.139
	X	0.639	0.022	0.285	0.140	0.098
dimer3	V	0.680	0.000	0.048	0.018	0.014
	X	0.816	0.000	0.047	2.9×10^{-5}	2.4×10^{-7}

V dimers explains the lack of efficient SF in vapor-grown crystals of DPT. Thus, based on the couplings alone, one would expect that $S_1 \rightarrow {}^1$ME rates will be larger in X. For dimer1, E_{stt} also favors the X form; however, in dimer2 SF is more exothermic in the V form (by ~0.06 eV). However, dimer3 has several orders of magnitude larger couplings (for both S_1 and S_1') in the V form. Thus, dimer3 will only contribute toward the total rate in V; however, its contribution is expected to be less that those of dimer1 and dimer2.

The relative rates are summarized in Table 6. As expected from the observed trends in couplings, the X form shows 50

Table 6. Relative Rates Computed for Different Dimers from V and X Structures at Different Temperatures

form	dimer	$S_1 \rightarrow {}^1$ME rate	$S_{1'} \rightarrow {}^1$ME rate	total rate
		T = 298 K		
V	1:2:3	1:14.3:1.77	1:0.58:0.006	1:459:1.86
X	1:2:3	1:2:0.006	$1:1.27:7.28 \times 10^{-7}$	1:2:0.005
V/X	1	1:368	1:11.1	1:133
V/X	2	1:51.3	1:24.2	1:0.58
V/X	3	1:1.16	1:0.001	1:0.35
V/X	all	1:49.5	1:15.7	1:0.86
		T = 77 K		
V	1:2:3	$1:4.11 \times 10^4$:220	7 858:197:1	$1:3.48 \times 10^6$:255
X	1:2:3	1:12:199	$1:0.052:2.84 \times 10^{-10}$	1:12:199
V/X	1	1:2 617	$1:1.21 \times 10^6$	1:2 617
V/X	2	1:0.77	$1:2.51 \times 10^6$	1:0.009
V/X	3	1:2 366	1:2.71	1:2 042
V/X	all	1:50.5	$1:1.25 \times 10^6$	1:0.61

times faster r_1 for the $S_1 \rightarrow {}^1$ME transition than the V form. Interestingly, the $S_{1'} \rightarrow {}^1$ME rate is also faster in X. However, the Boltzmann-averaged rates become nearly equal in the both forms, slightly favoring V. This reversal of the trend is due to large differences in E_d in dimer2. Whereas E_d in dimer2 from the V form is very small (as expected for half-integer ring offset structures), it is significant for the X form. Thus, it makes the contribution of the $S_{1'} \rightarrow {}^1$ME transition significant in V but not in X. This, combined with contributions from dimer3, reverses the ratio. Thus, although electronic couplings are clearly more favorable in X, the overall rates appear to be close in both forms. We note that this result depends strongly on the computed Davydov's splitting. Unlike for DPBF, our model predicts that the temperature dependence of the V/X rates ratio is weak. To summarize, our calculations predict small difference in SF rates in the two forms of DPT at all temperatures. However, given the uncertainties in the computed values and the strong effect of E_d on the ratio, the X form may show faster SF rate than the V form, owing to more favorable couplings in the former. Note that given inefficient SF in V, it is unlikely that the SF rate in X would become as fast as in the amorphous DPT.[23] It would be extremely interesting to measure SF rates in the two forms experimentally; such measurements will aid further development of the theoretical framework.

5. CONCLUSIONS

We investigate the SF process in three different compounds, DPBF, DPH, and DPT. Each compound forms two different types of molecular crystals. Although the polymorphs exhibit very similar structural, physical, and spectroscopic properties, the efficiency of SF is different, as illustrated by the experimental studies[25,26,28] of DPBF and DPH. We conducted electronic structure calculations of relevant electronic factors and estimated relative rates of the first step of SF using a simple kinetic model.[19] The computed ratios are in a good agreement with the experimental results for DPBF and DPH, which further validates our theoretical framework.[18,19] The analysis of the calculations reveals that (i) there is more than one pair of adjacent chromophores that contribute to SF; (ii) not only slip-stacked configurations show efficient fission; (iii) larger couplings can be explained by orbital delocalization and efficient mixing of the CR configurations into the ^{1}ME state (and, to a smaller extent, to S_1); and (iv) both electronic couplings and energies are responsible for different rates. Notably, the recent study of Van Voorhis and co-workers[20] has arrived at the same conclusion, that the thermodynamic drive (overall exothermicity of the singlet fission) plays a crucial role in determining the rates of the process.

The calculations also explain the increased difference of the rates in the DPBF polymorphs at low temperature; this is due to the difference in electronic energy gaps between the singlet and triplet states in the two crystal forms. In DPH, both couplings and E_{stt} contribute to the difference; the model predicts similar temperature dependence as in DPBF. For DPT, our model predicts similar rates for the two forms, although the X form features much more favorable electronic couplings. We note that relatively small changes in E_d for DPT may change

dx.doi.org/10.1021/jp505942k | J. Phys. Chem. C 2014, 118, 19608−19617

this conclusion in favor of faster SF in the X form. The combination of calculations and experimental measurements of rates and yields in various polymorphs at different temperatures will help to further understand the relative importance of different factors contributing to the efficiency of SF.

■ ASSOCIATED CONTENT

Supporting Information

Computational details, relevant Cartesian geometries, definitions of the scans, and additional results. This material is available free of charge via the Internet at http://pubs.acs.org.

■ AUTHOR INFORMATION

Corresponding Author

*E-mail: krylov@usc.edu.

Notes

The authors declare no competing financial interest.

■ ACKNOWLEDGMENTS

Support for this work was provided by the Center for Energy Nanoscience, an Energy Frontier Research Center funded by the U.S. Department of Energy, Office of Science, Office of Basic Energy Sciences (DE-SC0001013), and through the Scientific Discovery through Advanced Computing (SciDAC) program funded by U.S. Department of Energy, Office of Science, Advanced Scientific Computing Research and Basic Energy Sciences. A. B. K. acknowledges the support from the Welch Foundation (grant C-1559). A. B. K. was also supported in part by the National Science Foundation under Grant No. NSF PHY11-25915 during his stay at KITP program at University of California Santa Barbara. We are grateful to Prof. Josef Michl from University of Colorado, Boulder, for stimulating discussions and sharing his results prior to publication.

■ REFERENCES

(1) Smith, M. B.; Michl, J. Singlet Fission. *Chem. Rev.* **2010**, *110*, 6891−6936.

(2) Smith, M. B.; Michl, J. Recent Advances in Singlet Fission. *Annu. Rev. Phys. Chem.* **2013**, *64*, 361−368.

(3) Singh, S.; Jones, W. J.; Siebrand, W.; Stoicheff, B. P.; Schneider, W. G. Laser Generation of Excitons and Fluorescence in Anthracene Crystals. *J. Chem. Phys.* **1965**, *42*, 330−342.

(4) Johnson, J. C.; Nozik, A. J.; Michl, J. The Role of Chromophore Coupling in Singlet Fission. *Acc. Chem. Res.* **2013**, *46*, 1290−1299.

(5) Zimmerman, P. M.; Musgrave, C. B.; Head-Gordon, M. A Correlated Electron View of Singlet Fission. *Acc. Chem. Res.* **2013**, *46*, 1339−1347.

(6) Kuhlman, T. S.; Kongsted, J.; Mikkelsen, K. V.; Møller, K. B.; Sølling, T. I. Interpretation of the Ultrafast Photoinduced Processes in Pentacene Thin Films. *J. Am. Chem. Soc.* **2010**, *132*, 3431−3439.

(7) Zimmerman, P. M.; Bell, F.; Casanova, D.; Head-Gordon, M. Mechanism for Singlet Fission in Pentacene and Tetracene: From Single Exciton to Two Triplets. *J. Am. Chem. Soc.* **2011**, *133*, 19944−19952.

(8) Darancet, S.; Sharifzadeh, P.; Kronik, L.; Neaton, J. B. Low-Energy Charge-Transfer Excitons in Organic Solids from First-Principles: The Case of Pentacene. *J. Phys. Chem. Lett.* **2013**, *4*, 2917−2201.

(9) Havenith, R. W. A.; de Gier, H. D.; Broer, R. Explorative Computational Study of the Singlet Fission Process. *Mol. Phys.* **2012**, *110*, 2445−2454.

(10) Congreve, D. N.; Lee, J.; Thompson, N. J.; Hontz, E.; Yost, S. R.; Reusswig, P. D.; Bahlke, M. E.; Reineke, S.; Van Voorhis, T.; Baldo, M. A. External Quantum Efficiency Above 100% in a Singlet-Exciton-Fission-Based Organic Photovoltaic Cell. *Science* **2013**, *340*, 334−337.

(11) Vallett, P. J.; Snyder, J. L.; Damrauer, N. H. Tunable Electronic Coupling and Driving Force in Structurally Well Defined Tetracene Dimers for Molecular Singlet Fission: A Computational Exploration Using Density Functional Theory. *J. Phys. Chem. A* **2013**, *117*, 10824−10838.

(12) Casanova, D. Electronic Structure Study of Singlet-Fission in Tetracene Derivatives. *J. Chem. Theory Comput.* **2013**, *10*, 324−334.

(13) Beljonne, D.; Yamagata, H.; Brédas, J. L.; Spano, F. C.; Olivier, Y. Charge-Transfer Excitations Steer the Davydov Splitting and Mediate Singlet Exciton Fission in Pentacene. *Phys. Rev. Lett.* **2013**, *110*, 226402.

(14) Zeng, T.; Hoffmann, R.; Ananth, N. The Low-Lying Electronic States of Pentacene and Their Roles in Singlet Fission. *J. Am. Chem. Soc.* **2014**, *136*, 5755−5764.

(15) Mou, W.; Hattori, S.; Rajak, P.; Shimojo, F.; Nakano, A. Nanoscopic Mechanisms of Singlet Fission in Amorphous Molecular Solid. *Appl. Phys. Lett.* **2013**, *102*, 173301.

(16) Berkelbach, T. C.; Hybertsen, M. S.; Reichman, D. R. Microscopic Theory of Singlet Exciton Fission. I. General Formulation. *J. Chem. Phys.* **2012**, *138*, 114102.

(17) Akimov, A. V.; Prezhdo, O. V. Nonadiabatic Dynamics of Charge Transfer and Singlet Fission at the Pentacene/C_{60} Interface. *J. Am. Chem. Soc.* **2014**, *136*, 1599−1608.

(18) Feng, X.; Luzanov, A. V.; Krylov, A. I. Fission of Entangled Spins: An Electronic Structure Perspective. *J. Phys. Chem. Lett.* **2013**, *4*, 3845−3852.

(19) Kolomeisky, A. B.; Feng, X.; Krylov, A. I. A Simple Kinetic Model for Singlet Fission: A Role of Electronic and Entropic Contributions to Macroscopic Rates. *J. Phys. Chem. C* **2014**, *118*, 5188−5195.

(20) Yost, S. R.; Lee, J.; Wilson, M. W. B.; Wu, T.; McMahon, D. P.; Parkhurst, R. R.; Thompson, N. J.; Congreve, D. N.; Rao, A.; Johnson, K.; Sfeir, M. Y.; Bawendi, M. G.; Swager, T. M.; Friend, R. H.; Baldo, M. A.; Van Voorhis, T. A Transferable Model for Singlet-Fission Kinetics. *Nat. Chem.* **2014**, *6*, 492−497.

(21) Wu, Q.; Cheng, C.; Van Voorhis, T. Configuration Interaction Based on Constrained Density Functional Theory: A Multireference Method. *J. Chem. Phys.* **2007**, *127*, 164119.

(22) Müller, A. M.; Avlasevich, Y. S.; Schoeller, W. W.; Klausüllen; Bardeen, C. J. Exciton Fission and Fusion in Bis(tetracene) Molecules with Different Covalent Linker Structures. *J. Am. Chem. Soc.* **2007**, *129*, 14240−14250.

(23) Roberts, S. T.; McAnally, R. E.; Mastron, J. N.; Webber, D. H.; Whited, M. T.; Brutchey, R. L.; Thompson, M. E.; Bradforth, S. E. Efficient Singlet Fission Found in a Disordered Acene Film. *J. Am. Chem. Soc.* **2012**, *134*, 6388−6400.

(24) Ramanan, C.; Smeigh, A. L.; Anthony, J. E.; Marks, T. J.; Wasielewski, M. R. Competition Between Singlet Fission and Charge Separation in Solution-Processed Blend Films of 6,13-Bis(triisopropylsilylethynyl)pentacene with Sterically-Encumbered Perylene-3,4:9,10-bis(dicarboximide)s. *J. Am. Chem. Soc.* **2012**, *134*, 386−397.

(25) Johnson, J. C.; Nozik, A. J.; Michl, J. High Triplet Yield from Singlet Fission in a Thin Film of 1,3-Diphenylisobenzofuran. *J. Am. Chem. Soc.* **2010**, *132*, 16302−16303.

(26) Ryerson, J.; Schrauben, J. N.; Ferguson, A. J.; Sahoo, S. C.; Naumov, P.; Havlas, Z.; Michl, J.; Nozik, A. J.; Johnson, J. C. Two Thin Film Polymorphs of the Singlet Fission Compound 1,3-Diphenylisobenzofuran. *J. Phys. Chem. C* **2014**, *118*, 12121−12132.

(27) Schrauben, J. N.; Ryerson, J.; Michl, J.; Johnson, J. C. The Mechanism of Singlet Fission in Thin Films of 1,3-Diphenylisobenzofuran. *J. Am. Chem. Soc.* **2014**, *136*, 7363−7373.

(28) Dillon, R. J.; Piland, G. B.; Bardeen, C. J. Different Rates of Singlet Fission in Monoclinic Versus Orthorhombic Crystal Forms of Diphenylhexatriene. *J. Am. Chem. Soc.* **2013**, *135*, 17278−17281.

(29) Walker, B. J.; Musser, A. J.; Beljonne, D.; Friend, R. H. Singlet Exciton Fission in Solution. *Nat. Chem.* **2013**, *5*, 1019−1024.

(30) Kitamura, C.; Matsumoto, C.; Kawatsuki, N.; Yoneda, A.; Kobayashi, T.; Naito, H. Crystal Structure of 5,12-Diphenyltetracene. *Anal. Sci. Soc. Jpn.* **2006**, *22*, x5−x6.
(31) Johnson, R. C.; Merrifield, R. E. Effects of Magnetic Fields on the Mutual Annihilation of Triplet Excitons in Anthracene Crystals. *Phys. Rev. B* **1970**, *1*, 896−902.
(32) Anslyn, E. V.; Dougherty, D. A. *Modern Physical Organic Chemistry*; University Science Books: Herndon, VA, 2006.
(33) Streidl, N.; Denegri, B.; Kronja, O.; Mayr, H. A Practical Guide for Estimating Rates of Heterolysis Reactions. *Acc. Chem. Res.* **2010**, *43*, 1537−1549.
(34) Rosta, E.; Warshel, A. Origin of Linear Free Energy Relationships: Exploring the Nature of the Off-Diagonal Coupling Elements in S_{N2} Reactions. *J. Chem. Theory Comput.* **2012**, *8*, 3574−3585.
(35) Chan, W.-L.; Ligges, M.; Zhu, X.-Y. The Energy Barrier in Singlet Fission Can Be Overcome through Coherent Coupling and Entropic Gain. *Nat. Chem.* **2012**, *4*, 840−845.
(36) Matsika, S.; Feng, X.; Luzanov, A. V.; Krylov, A. I. What We Can Learn from the Norms of One-Particle Density Matrices, and What We Can't: Some Results for Interstate Properties in Model Singlet Fission Systems. *J. Phys. Chem. A* **2014**, DOI: 10.1021/jp506090g.
(37) Prezhdo, O. V.; Rossky, P. J. Evaluation of Quantum Transition Rates from Quantum-Classical Molecular Dynamics Simulations. *J. Chem. Phys.* **1997**, *107*, 5863−5878.
(38) Izmaylov, A. F.; MendiveTapia, D.; Bearpark, M. J.; Robb, M. A.; Tully, J. C.; Frisch, M. J. Nonequilibrium Fermi Golden Rule for Electronic Transitions through Conical Intersections. *J. Chem. Phys.* **2011**, *135*, 234106.
(39) Lee, M. H.; Dunietz, B. D.; Geva, E. Calculation from First Principles of Intramolecular Golden-Rule Rate Constants for Photo-Induced Electron Transfer in Molecular DonoAcceptor Systems. *J. Phys. Chem. C* **2013**, *117*, 23391−23401.
(40) vanKampen, N. G. *Stochastic Processes in Physics and Chemistry*, 3rd ed.; Elsevier: North Holland, 2001.
(41) Casanova, D.; Slipchenko, L. V.; Krylov, A. I.; Head-Gordon, M. Double Spin-Flip Approach within Equation-of-Motion Coupled Cluster and Configuration Interaction Formalisms: Theory, Implementation and Examples. *J. Chem. Phys.* **2009**, *130*, 044103.
(42) Bell, F.; Zimmerman, P. M.; Casanova, D.; Goldey, M.; Head-Gordon, M. Restricted Active Space Spin-Flip (RAS-SF) with Arbitrary Number of Spin-Flips. *Phys. Chem. Chem. Phys.* **2013**, *15*, 358−366.
(43) Dunning, T. H. Gaussian Basis Sets for Use in Correlated Molecular Calculations. I. The Atoms Boron through Neon and Hydrogen. *J. Chem. Phys.* **1989**, *90*, 1007−1023.
(44) Shao, Y.; Fusti-Molnar, L.; Jung, Y.; Kussmann, J.; Ochsenfeld, C.; Brown, S.; Gilbert, A. T. B.; Slipchenko, L. V.; Levchenko, S. V.; O'Neill, D. P.; et al. Advances in Methods and Algorithms in a Modern Quantum Chemistry Program Package. *Phys. Chem. Chem. Phys.* **2006**, *8*, 3172−3191.
(45) Krylov, A. I.; Gill, P. M. W. Q-Chem: An Engine for Innovation. *WIREs Comput. Mol. Sci.* **2013**, *3*, 317−326.